Global regulatory factor AaLaeA upregulates the production of antitumor substances in endophytic Alternaria alstroemeria

Xuemin Yin
Long Han
Wen Zheng
Lu Cai
Min Qin
Zhangjiang He (zjhe3@gzu.edu.cn)
Jichuan Kang

Research Article

Keywords: Endophytic fungi, A. alstroemeria, LaeA, Antitumor, Transcriptome and metabolome

Posted Date: June 16th, 2022

DOI: https://doi.org/10.21203/rs.3.rs-1721421/v1

Abstract

The global regulatory factor LaeA has been shown to be involved in the biosynthesis of secondary metabolites in various fungi. In a previous work, we isolated an endophytic fungus from *Artemisia annua*, and its extract had a significant inhibitory effect on the A549 cancer cell line. Phylogenetic analysis based on ITS sequences further identified the strain as *Alternaria alstroemeria.* Overexpression of the global regulatory factor *AalaeA* gene resulted in significantly increased antitumor activity of this strain's extract. The 3 - (4, 5- dimethylthiazol − 2 - yl) -2, 5 - diphenyltetrazolium bromide (MTT) assay results showed that the inhibition rate of the *AalaeA*^{OE29} mutant extract on A549 cancer cells was significantly higher than that of the WT extract, as the IC_{50} decreased from 195.0 μg/mL to 107.4 μg/mL, and the total apoptosis rate was enhanced. Overexpression of the *AalaeA* gene significantly increased the contents of myricetin, geraniol, ergosterol and 18 other antitumor compounds as determined by metabolomic analysis. Transcriptomic analysis revealed significant changes in 95 genes in the mutant strain, including polyketide synthases (PKSs), nonribosomal peptide synthases (NRPSs), cytochrome P450s, glycosyltransferases (GTs), acetyl-CoA acetyltransferases and others. These results suggested that AaLaeA mediated the antitumor activity of the metabolites in *A. alstroemeria* by regulating multiple metabolic pathways.

Introduction

Endophytic fungi are interesting microorganisms that colonize the healthy internal tissues of living plants without causing any symptoms of disease (Christian et al., 2020). Complicated interactions gradually form in the symbiotic process that lead the fungus to be able to synthesize secondary metabolites that are identical or similar to those produced by the host plant (Yan et al., 2018; Ancheeva et al., 2020). Endophytic fungi produce many promising anticancer compounds, such as paclitaxel, camptothecin, and vinblastine, which can be purified and isolated from the fungi (Hridoy et al., 2022). The endophytic fungi *Alternaria* spp. has gained increasing attention due to the extensive bioactivity of its abundant secondary metabolites. For example, one cephalotaxus alkaloid and four bioflavonoids isolated from *A. alternata* were found to show pronounced cytotoxicity against A549, NCI-H460, and HL60 cancer cells (Ma et al., 2020). Two cyclopentaisochromenes from *Alternaria* sp. TNXY-P-1 exhibited antitumor activity against the cancer cell line HL-60 (Lu et al., 2018). Dibenzo-α-pyrones isolated from *Alternaria* sp. Samif01 showed antibacterial and antioxidant activity (Tian et al., 2017). Therefore, it is meaningful to conduct research on the secondary metabolites of *Alternaria* spp.

However, fungal production of secondary metabolites is restrained under laboratory conditions (Shwab *et al.*, 2008). LaeA, a major global regulator in filamentous fungi, was first identified in *Aspergillus nidulans*, and the cDNA sequence revealed a conserved S-adenosylmethionine binding site in the middle of the coding region (Bok *et al.*, 2004). This finding indicated that LaeA was involved in DNA methylation, which is the most well-studied form of epigenetic modification. Epigenetic modification has been suggested to be related to the control of the expression of fungal biosynthetic pathways and the production of metabolites (Williams et al., 2008). LaeA was shown to be involved in the biosynthesis of secondary

metabolites in various fungi, including *Penicillium chrysogenum*, *Fusarium verticillioides*, and *Chaetomium globosum*, which implied that LaeA had a conserved function in fungi (Martín *et al*., 2016; Butchko et al., 2012; Jiang et al., 2016). As a positive global regulator in a wide range of filamentous fungi, overexpression of LaeA not only increased the production of known compounds, such as monacolin K and cyclopiazonic acid, but also led to the identification of new compounds (Zhang et al., 2020; Hong *et al*., 2016; Yu et al., 2019), which indicated that overexpression of LaeA was an important means to enhance the secondary metabolites in filamentous fungi.

In our early study, endophytic *A. alstroemeria* ZZ-HY-03-02 was isolated from the medicinal plant *Artemisia annua*, and its extract had a significant inhibitory effect on the A549 cancer cell line. However, it is unknown whether overexpression of the *laeA* gene mediated its antitumor activity. In our study, we overexpressed *AalaeA* gene in this strain, evaluated the antitumor activity of its extract and explored the alterations in the corresponding substances and genes during this process *via* combined analyses of metabolomics with transcriptomics. Our research provides a reference to further study the regulation of secondary metabolism of *A. alstroemeria* by AaLaeA.

Materials And Methods

Strain identification and AalaeA gene cloning

The isolated and purified strain ZZ-HY-03-02 used in this study was available at the Southwest Biomedical Resources of the Ministry of Education under accession number SBRME996294. The strain was cultured on a PDA plate in a 28°C incubator for 6 days. The morphological characteristics of the colony, conidiophores and conidia were observed using an optical microscope to conduct preliminary strain identification (CKX53, Olympus, Tokyo, Japan).

Fungal genomic DNA was extracted from mycelia cultured in 500 mL of liquid Sabourand medium with shaking at 180 rpm at 28°C for 7 days. After cultivation, the mycelia were collected, quickly frozen in liquid nitrogen, ground and used to extract genomic DNA according to a fungal DNA kit (Omega Bio-Tek, Georgia, USA). The ITS sequence was amplified with primers ITS4 and ITS5 using genomic DNA as a template. To identify homologies, the sequenced ITS sequence was blasted on the NCBI website (http://www.ncbi.nlm.nih. gov/), and sequences showing high homology were downloaded. Multiple sequence alignment was performed using the Clustal W alignment algorithm, and a phylogenetic tree was constructed using the maximum likelihood method in MEGA 7.0 with 1000 bootstrap replicates. Similarly, the *laeA* gene of *A. alternata* was used as a template to design primers to amplify the homologous *laeA* gene of *A. alstroemeria to* identify AaLaeA. The open reading frame encoding the *laeA* gene *of A. alstroemeria* was amplified using *laeA*-F and *laeA*-R. The protein sequence was blasted, and a phylogenetic tree was constructed to identify LaeA in *A. alstroemeria*.

Acquisition of overexpression mutants

The *PtrpC* promoter from *Aspergillus nidulans* was selected to drive the expression of the *AalaeA* gene. The *AalaeA* and *PtrpC* sequences were amplified using *A. alstroemeria* genomic DNA and the pK_2*hyg* plasmid (constructed in our previous study, He et al. 2017) as templates, respectively. The two PCR products were fused, and the DNA fragment containing *AalaeA* was then ligated into the corresponding site of the pK_2*hyg* plasmid (first digested with HandIII and XbaI) using recombinant ligase (Novizan Biotechnology Co., Ltd., Nanjin, China). The constructed pK_2*hyg-PtrpC-AalaeA* vector was mobilized into *A. tumefaciens* strain AGL-1 via electrotransformation. *A. tumefaciens* strain AGL-1 harbouring the T-DNA binary vector was introduced into the conidia of the wild-type (WT) strain. The transformation protocol was a modification of the method developed by Estiarte *et al*. (Estiarte et al., 2016). *A. tumefaciens* strain AGL-1 harbouring the T-DNA binary vector was cultivated for 20 h in 20 mL of YEB (0.1% (w/v) yeast extract, 0.05% (w/v) $MgSO_4.7H_2O$, 0.5% (w/v) sucrose, 1% (w/v) tryptone) liquid medium containing kanamycin (50 μg/mL) and carbenicillin (50 μg/mL). The *A. tumefaciens* cells were collected, and then IM liquid medium (0.3‰ (w/v) $MgSO_4{\cdot}7H_2O$, 0.3‰ (w/v) NaCl, 0.78% (w/v) MES, 0.3‰ (w/v) K_2HPO_4, 0.5% (v/v) glycerol, pH 5.3) supplemented with 400 μmol/L acetosyringone and 10 mmol/L glucose was added. The OD_{660} value of the medium was adjusted to 0.15, and the cells were incubated at 28°C and 180 rpm for 6 h in the dark. Mycelia cultured for 12 days on a PDA plate were scraped and placed into a centrifuge tube, and 0.05% (w/v) Tween-80 solution was added followed by shaking and filtering to obtain conidia. The conidia were adjusted to a concentration of 1×10^6 and mixed with *A. tumefaciens* cells at a ratio of 1:1. The mixture was spread over nitrocellulose membrane filters on agar IM medium (containing 200 μmol/L acetosyringone and 5 mmol/L glucose). After cocultivation at 26°C for 48 h, the membranes were transferred to CZM agar plates (0.2% (w/v) $NaNO_3$, 3% (w/v) sucrose, 0.1% (w/v) K_2HPO_4, 0.0001% $FeSO_4.7H_2O$, 0.05 (w/v) KCl, 0.05% (w/v) $MgSO_4.7H_2O$, pH 7.0) containing 100 μg/mL hygromycin B (Shanghai Bioengineering Co., Ltd., Shanghai, China) as a selection agent and 200 μg/mL cefotaxime (Shanghai Bioengineering Co., Ltd., Shanghai, China) to inhibit the growth of *A. tumefaciens* cells. The single transformant was transferred to CZM agar supplemented with 100 μg/mL hygromycin B for purification.

Total RNA was isolated from the mycelia with an RNApure Tissue & Cell Kit (Kangwei Century Biological Technology Co., Ltd., Jiangsu, China) and reverse transcribed into cDNA with a StarScript II reverse transcription kit according to the manufacturer's instructions (Genestar, Beijing, China). The qRT–PCR amplifications were performed on a Bio–Rad CFX96 real-time PCR system C1000 thermal cycler (Bio–Rad, Hercules, CA, USA). The qRT–PCR protocol consisted of initial denaturation at 95°C for 5 min, denaturation at 95°C for 30 s, annealing at 56°C for 30 s, and extension at 72°C for 45 s (40 cycles). mRNA expression was normalized to *actin* (Nishikawa, *et al*., 2013), and the data were calculated using the $2^{-\triangle\triangle Ct}$ method. All primer sequences used for the construction of the overexpression mutant are shown in Table S1.

Preparation of the extracts

The concentrations WT and *AalaeA*^{OE29} conidia were adjusted to 1×10^6, and then 4 mL of each was added to 500 mL of liquid Sabourand medium (the ratio of glucose to peptone was 4:1). Then, fermentation was carried out by cultivation at 180 rpm on a shaker at 28°C for 7 days. After fermentation, the cultures were filtered. Fluids were extracted using ethyl acetate (proportion 1:1) three times, while the mycelia were stored at -80°C after quick freezing with liquid nitrogen. The extracts were dried in a rotary evaporator (R-200; Buchi, Flawil, Switzerland) at 38°C and dissolved in 1 mL of dimethyl sulfoxide (DMSO).

MTT and annexin V-FITC/PI

Cells were incubated in RPMI 1640 medium (Beijing Solarbio Science & Technology Co., Ltd., Beijing, China) containing 10% foetal bovine serum (Gibco BRL, Grand Island, USA) and 1% penicillin–streptomycin solution (Gibco BRL, Grand Island, USA) at 37°C in a humidified incubator containing 5% CO_2 for 24 h. Then, cells in the logarithmic phase were seeded into 96-well plates at a concentration of 1×10^5 cells/well for 24 h of incubation. The medium was then removed, and 100 μL of medium containing five different concentrations of doxorubicin (ADM) and extracts of the WT and *AalaeA*^{OE29} strains were added to different wells. Different drug concentrations were diluted with RPMI 1640 medium to ensure that the DMSO content was less than 0.1%. Following incubation for 48 h, 20 μL of MTT was added to culture for another 4 h. Subsequently, the medium containing MTT was removed and 150 μL of DMSO was added to each well accompanied by low-speed oscillation for 10 min to dissolve the crystals. The absorbance was measured at 490 nm with a microplate reader (Bio–Rad Laboratories, Hercules, CA, USA). The relative inhibition rates were calculated as follows: relative inhibition rate (%) = (OD value of the negative control-OD value of ADM/extracts added group)/(OD value of the negative control) ×100%.

Similarly, cells were inoculated at a concentration of 1×10^6 in 6-well plates and treated with different concentrations of the extracts for 48 h. The cells were then collected and the medium was transferred to a centrifuge tube and centrifuged. The cells were rinsed with PBS twice and stained with annexin V/PI following the instructions of the Annexin V-FITC Apoptosis Detection Kit (Beijing Solarbio Science & Technology Co., Ltd., Beijing, China). Cell apoptosis was detected by flow cytometry (Thermo Fisher Scientific; Carlsbad, CA, USA).

Transcriptome and metabolome analyses

The extracts and mycelia (cultured in liquid Sabourand medium at 180 rpm on a shaker at 28°C for 7 days) were quickly frozen in liquid nitrogen and sent to Baimaike (https: // international. biocloud. net / zh / user / login) for transcriptomic and metabolomic analyses.

Nontarget LC–MS/MS metabolome detection was carried out with a Waters Xevo G2-XS QTOF high-resolution mass spectrometer, which can collect primary and secondary mass spectrometry data in MSe mode under the control of the acquisition software (MassLynx V4.2, Waters). In each data acquisition cycle, dual-channel data acquisition can be performed with both low collision energy and high collision energy at the same time. The low collision energy was 2 V, the high collision energy range was 10 ~ 40 V,

and the scanning frequency was 0.2 seconds for each mass spectrum. The parameters of the ESI source were as follows: capillary voltage, 2000 V (positive ion mode) or -1500 V (negative ion mode); cone voltage, 30 V; ion source temperature, 150°C; drying gas temperature, 500°C; backflush gas flow rate, 50 L/h; and drying gas flow rate, 800 L/h.

The purity, concentration and integrity of the RNA samples were examined using advanced molecular biology equipment to ensure the use of qualified samples for transcriptome sequencing. A total amount of 1 μg of RNA per sample was used as the input material for RNA sample preparations. Sequencing libraries were generated using the NEBNext®Ultra™ RNALibrary Prep Kit for Illumina® (NEB, USA) following the manufacturer's protocol, and index codes were added to attribute the sequences to each sample. Briefly, mRNA was purified from total RNA using poly-T oligo-attached magnetic beads. Fragmentation was carried out using divalent cations under elevated temperature in NEBNext First Strand Synthesis Reaction Buffer (5X). First-strand cDNA was synthesized using random hexamer primers and M-MuLV Reverse Transcriptase. Second-strand cDNA synthesis was subsequently performed using DNA Polymerase I and RNase H. Remaining overhangs were converted into blunt ends *via* exonuclease/polymerase activities. After adenylation of the 3' ends of the DNA fragments, NEBNext Adaptor with hairpin loop structure was ligated to prepare for hybridization. To preferentially select cDNA fragments 240 bp in length, the library fragments were purified with an AMPure XP system (Beckman Coulter, Beverly, USA). Then, 3 μl of USER enzyme (NEB, USA) was used with size-selected, adaptor-ligated cDNA at 37°C for 15 min followed by 5 min at 95°C before PCR. Then, PCR was performed with Phusion High-Fidelity DNA polymerase, universal PCR primers and Index (X) Primer. Finally, the PCR products were purified (AMPure XP system), and library quality was assessed on an Agilent Bioanalyzer 2100 system. Clustering of the index-coded samples was performed on a cBot Cluster Generation System using TruSeq PE Cluster Kit v3-cBot-HS (Illumina) according to the manufacturer's instructions. After cluster generation, the library preparations were sequenced on an Illumina HiSeq 2000 platform and paired-end reads were generated.

The resequencing analyses were commissioned to Sangon Biotech (https : // www. sangon. com/). The description of the method refered to Zhang *et al.* (Zhang et al., 2021).

Statistical analysis

The qRT–PCR results were analysed by analysis of variance (ANOVA). Student's t test was used for antitumor activity and apoptosis by flow cytometry analyses of each sample. Data are expressed as the mean ± SD, and $P < 0.05$ was considered statistically significant. SPSS 12.0 software was used for statistical analysis of the IC_{50} values. After the metabolomics and transcriptomics analyses were performed, the genes and metabolites that met the criteria of FC (fold change difference multiple) ≥ 1, FDR (false discovery rate) ≤ 0.05, VIP (variable projection significance assessment) > 1.0 or FC ≥ 1, $P < 0.05 \leq 0.05$, and VIP > 1.0 were considered differentially expressed genes (DEGs) or candidate metabolites.

Results

A. alstroemeria extract inhibited the proliferation of A549 cancer cells

To determine whether *A. alstroemeria* had antitumor activity, an MTT assay was carried out to detect the sensitivity of the A549 cancer cell line to the extract. First, ADM was used as a positive control to detect the state of the cell. The inhibition rate after ADM treatment increased significantly with gradually increasing concentrations (Fig. 1A). The IC_{50} was 2.06 μg/mL, which was consistent with previous studies (Xie et al., 2015; Zhu et al., 2012). The results showed that A549 cancer cells grew normally and could be used for further study. Subsequently, we found that treatment with the extract led to significantly increased inhibition of cell proliferation. The relative inhibition rate reached 59% at 300 μg/mL extract (Fig. 1B), which suggested that the extract produced a clear inhibitory effect on the A549 cancer cell line.

Figure 1. Effects of ADM and A. alstroemeria extract on the A549 cancer cell line. A549 cancer cells were seeded at a density of 1×105 cells/well and treated with different concentrations of ADM or A. alstroemeria extract for 48 h; three replicates were performed for each concentration. An MTT assay was conducted to determine the cellular proliferation inhibition rate. A. Relative inhibition rates of A549 cancer cells after treatment with 0.625, 1.25, 2.5, 5 and 10 μg/mL ADM. Each point on the graph represents the mean ± SD of triplicate tests. B. Relative inhibition rates of A549 cancer cells after treatment with 18.75, 37.5, 75, 150 and 300 μg/mL extract. Values represent the mean ± SD of 3 replicates per treatment.

To identify the strain ZZ-HY-03-02, we observed the morphological characteristics of the strain. Round and caesious colonies with neat edges were seen, grey–brown mycelia with white aerial mycelia on the colony surface developed (Fig. 2A), and a yellowish-black pigment was produced on the back (Fig. 2B). The vegetative hyphae were brown, branched, and septate, and the conidiophores were single and straight (Fig. 2C). The conidia were obclavate or ellipsoid, pale brown or brown–black, with 1–3 transverse septa (Fig. 2D) with lengths ranging from 13.4-126.1 μm. The morphological characteristics of the strain were similar to those of *Alternaria* spp. Phylogenetic analysis based on the ITS sequence further suggested that ZZ-HY-03-02 showed the closest homology to *A. alstroemeria*, with 100% similarity. Therefore, the strain was identified as *A. alstroemeria* (Fig. 2E).

AaLaeA mediated the antitumor activity of A. alstroemeria

To explore whether AaLaeA mediates the antitumor activity exhibited by the *A. alstroemeria* extract, the *laeA* protein-coding gene was first amplified. The results showed that the LaeA protein of *A. alstroemeria* displayed similarity (100% homology) with LaeA of *A. alternata*. Therefore, the protein was named AaLaeA (Fig. 3A, Fig. S1).

To obtain overexpression mutants of *AalaeA*, the original promoter of the *AalaeA* gene in the WT was replaced by the constitutive promoter *PtrpC* of *Aspergillus nidulans* (Fig. 3B) and introduced to the WT through Agrobacterium-mediated transformation. Then, 4 transformants were randomly selected for PCR verification by amplifying the hygromycin phosphotransferase (*hyg*) gene carried by the pK_2*hyg* vector.

The specific band of the transformants could be amplified at approximately 1000 bp, while the WT had no bands (Fig. 3C). The expression of *AalaeA* in *AalaeA*^{OE29} was 15-fold higher than that in the WT by qRT–PCR. (Fig. 3D) The growth of the WT and *AalaeA*^{OE29} strains on hygromycin B-resistant plates was observed. *AalaeA*^{OE29} grew normally, while WT growth was inhibited (Fig. 3E).

Cell proliferation, detected by MTT assays, and apoptosis analysis, assessed by annexin V-FITC/PI double staining, were investigated to study the differences in the antitumor properties of the *AalaeA*^{OE29} and WT extracts. The MTT results showed that the *AalaeA*^{OE29} extract showed significantly higher inhibition of A549 cancer cells than the WT extract, and the IC_{50} correspondingly decreased from 195.0 μg/mL to 107.4 μg/mL (Fig. 3F). The apoptosis results showed that at a concentration of 300 μg/mL, the total apoptosis rate of *A. alstroemeria* increased 1.56-fold (Fig. 3G, Fig. S2). These results suggested that AaLaeA mediated the antitumor effects of the extracts.

AaLaeA mediated the production of antitumor compounds

To explore the effects of AaLaeA on the metabolism of *A. alstroemeria*, nontargeted LC–MS/MS was applied to detect the metabolites of the WT and *AalaeA*^{OE29} strains. The identified metabolites that matched the criteria of FC > 1, $P < 0.05$ and VIP > 1 were defined as candidate metabolites. Principal component analysis (PCA) was used to analyse the differences in metabolites between the WT and *AalaeA*^{OE29} strains. PCA showed a large spread between the two groups with good agreement among the three replicates (Fig. 4A). Consistent with PCA, there was clear separation between WT and *AalaeA*^{OE29} in the orthogonal partial least squares discrimination analysis (OPLS-DA) model (Fig. 4B). The values of R2Y and Q2 were very close to 1, which indicated that the established model was well constructed and had precise predictability. A permutation test was used to evaluate the quality of the OPLS-DA model (Fig. 4C). The R2Y value was larger than that of Q2, and the Y-intercept was less than 0.05, indicating that the model did not show overfitting and could explain the difference between the two groups of samples well. A total of 860 metabolites were detected, of which 201 were downregulated, 431 were upregulated and 228 were unchanged (Fig. 4D). In general, the metabolites from the WT and *AalaeA*^{OE29} showed significant differences.

KEGG pathway enrichment analysis was conducted to further analyse the pathways affected by candidate metabolite production. The top 20 KEGG pathways (Fig. 5) included the biosynthesis and metabolism of amino acids (cysteine and methionine metabolism, valine biosynthesis and metabolism/degradation, etc.), lipid metabolism and biosynthesis (arachidonic acid metabolism, fatty acid biosynthesis, etc.), sugar metabolism (galactose metabolism, etc.), vitamin biosynthesis and metabolism (vitamin B6 metabolism, riboflavin metabolism, etc.), and protein-related pathways (ABC transporters). In addition, steroid biosynthesis and 2-oxycarboxylic acid enhancement were also enriched (Fig. 5). These results suggested that AaLaeA was involved in the biosynthesis of compounds in the corresponding pathways and that both secondary metabolism and basal metabolism in *A. alstroemeria* were significantly regulated by AaLaeA.

To identify the metabolites that caused the differences in antitumor activity between the WT and *AalaeA*^{OE29} extracts, the antitumor compounds involved in KEGG pathways were first screened, including lanosterol, ergosterol (ko00100), myricetin, epicatechin gallate (ko01110), geraniol, humulene, (2E,6E)-farnesol, (ko00909), AICAR, (ko01110), trans-cinnamic acid (ko00360, ko00998, ko01110, ko00130), cinnamaldehyde (ko01100), carnitine (ko02010, ko00310, ko01100) and L-methionine (ko01230, ko01100, ko00270, ko01210, ko01110, ko00970).

In addition, the candidate metabolites were further screened using FC > 1.5, $P < 0.05$ and VIP > 1 as selection criteria, and 6 compounds, including quercetin 3-O-glucuronide, engeletin, alstilbin, terpinen-4-ol, alpha-mangostin and matrine were selected. The classifications of the 18 reported potential antitumor compounds are shown in Table 1, including flavonoids myricetin (Anwar et al., 2022) and epicatechin gallate (Huang et al., 2016); flavonoid glycosides quercetin 3-O-glucuronide (Wu et al., 2018), alstilbin (Thuan et al., 2017) and engeletin (Liu et al., 2020); terpenoids (2E,6E)-farnesol (Jung et al., 2018), terpinen-4-ol (Wu et al., 2012), geraniol (Crespo et al., 2020) and humulene (Legault et al., 2003); alkaloids AICAR (Su et al., 2019), carnitine (Sun et al., 2020), and matrine (Pu et al., 2018); steroids ergosterol (Liu et al., 2019) and lanosterol (Chung et al., 2010); xanthone alpha-mangostin (Zhang *et al*., 2017); and amino acids and their derivatives, including L-methionine (Hassan *et al*., 2010), cinnamaldehyde (Wu et al., 2017) and trans-cinnamic acid (Tsai et al., 2013). Most of these compounds (13 out of 18) have been reported to directly inhibit the A549 cancer cell line with the exception of quercetin 3-O-glucuronide, (2E,6E)-farnesol, AICAR, L-methionine, and carnitine. However, these 5 compounds also possess antitumor properties or auxiliary functions in the treatment of cancer. Thus, the results showed that AaLaeA mediated the production of these antitumor compounds.

Table 1
18 antitumor compounds were significanly up-regulated.

Classification	Compounds	P value	VIP value	Log2FC
Flavonoid glycosides	Quercetin 3-O-glucuronide	0.001798176	1.08	36.5
	Alstilbin	0.000526126	1.08	7.5
	Engeletin	0.000583755	1.09	6.4
Flavonoids	Myricetin	0.000842403	1.09	28.6
	Epicatechin gallate	4.42E-08	1.09	5.0
Xanthone	Alpha-mangostin	0.006297392	1.06	13.1
Terpenoids	(2E,6E)-Farnesol	7.25E-07	1.09	2.7
	Terpinen-4-ol	0.0091504	1.06	2.6
	Geraniol	0.000192724	1.08	6.3
	Humulene	0.001032299	1.08	24.8
Steroids	Ergosterol	0.000740418	1.07	0.6
	Lanosterol	0.000146113	1.08	4.6
Alkaloids	Matrine	0.000508063	1.08	1.5
	Carnitine	1.70E-05	1.08	3.1
	AICAR	0.000243335	1.08	14.1
Amino acids and their derivatives	L-methione	4.63E-05	1.09	13.6
	Cinnamaldehyde	0.001461212	1.08	4.6
	trans-Cinnamic acid	0.000403149	1.07	1.0

AaLaeA mediated the expression of related genes to control the biosynthesis of antitumor compounds

Transcriptomic analysis was performed to identify the related genes of the WT and *AalaeA*^{OE29} strains that might be involved in the biosynthesis of antitumor compounds. Clean reads ranged from 20,815,809 – 25,630,558, with the percentage of Q30 being 93.69% or above and the GC ratio being greater than 54.05% (Table S2). These results indicated that the transcriptome data were qualified for use in subsequent analysis. A total of 3648 differentially expressed genes (DEGs), consisting of 1576 upregulated genes and 2072 downregulated genes, were identified (Fig. 6A). A total of 943 DEGs were involved in 120 KEGG pathways, which were classified into four main groups. A large proportion were

involved in “metabolism”, followed by “genetic information processing” and “cell process and environmental information processing” (Fig. 6B). The results suggested that AaLaeA was mainly involved in the metabolic processes of *A. alstroemeria.*

To identify the genes mediated by AaLaeA that might be involved in the synthesis of antitumor compounds, 66 possible related DEGs were first screened by integrating the GO and KEGG pathway enrichment analyses, of which PKSs, NRPSs, cytochrome P450s, ABC transporters, GTs, WD40 repeat-like proteins, Myb transcription factors and the isoflavone reductase family were screened and classified according to annotations by the NR, SWISS-PORT, and Pfam databases (Fig. 7A, Table S3). These genes were significantly upregulated or downregulated. For example, PKSA and the highly reducing polyketide synthase PKS2 were upregulated 12-fold and downregulated 22-fold, respectively. The WD40 repeat-like proteins were upregulated, and the highest expression of the upregulated cytochrome P450 reached 59-fold, while the lowest downregulated gene was 7-fold. Significantly, the isoflavone reductase family protein-like protein CipA was upregulated 126-fold, while the other isoflavone reductase family protein was downregulated 32-fold. In addition, 29 genes enriched in the biosynthesis of steroids (ko04070), terpenoids (ko04130), and biosynthesis of various secondary metabolites (ko00254) pathways were obtained from combined transcriptomic and metabolomic KEGG pathway analyses (Fig. S3). These genes included upregulated phosphomevalonate kinase 9, acetyl-CoA acetyltransferase, dehydrodolichyl diphosphate synthase, 3-keto-steroid reductase, putative sterol desaturase and sterol 24-C-methyltransferase, and downregulated C-8 sterol isomerase, hydroxymethylglutaryl-CoA synthase, thiolase and others. (Fig. 7B, Table S4). A fairly large number of these genes have been reported to be associated with the synthesis of secondary metabolites, such as terpenoids, sterols, alkaloids, and flavonoids. Consequently, we speculated that AaLaeA mediated 95 gene changes that might be involved in the synthesis of antitumor metabolic compounds in *A. alstroemeria.*

To verify the reproducibility and repeatability of the DEG identification from transcriptome sequencing, 8 upregulated and downregulated DEGs were selected and verified by qRT–PCR (Fig. 7C, Table S5). The expression trend was consistent with that of the transcriptomic analysis, indicating that the transcriptome data were relatively reliable.

Discussion

Endophytic fungi colonized in medicinal plants are capable of generating different bioactive secondary metabolites on account of their special niche, including those from their host plants that have important biological activities (El Hajj Assaf et al., 2020; Gómez *et al*., 2018). It has been shown that the putative methyltransferase LaeA suppresses or activates the expression of gene clusters, and its overexpression can induce the production of secondary metabolites (Macheleidt et al., 2016). Therefore, we overexpressed the *AalaeA* gene in *A. alstroemeria* isolated from the medicinal plant *Artemisia annua* and found that the antitumor effects of the mutant extract were significantly enhanced compared to those of the WT extract *via* the determination of A549 cancer cell proliferation and apoptosis.

The contents of many compounds with reported antitumor activity were significantly upregulated after overexpression of the *AalaeA* gene by further metabolomic analysis; these compounds mainly included flavonoids, terpenoids, alkaloids and others. Most of these compounds were reported to inhibit A549 cancer cells; for instance, it was reported that myricetin significantly inhibited the proliferation of and induced apoptosis in in these cells(Anwar et al., 2022). The flavonoid glycoside alstilbin was proven in a previous study to be a potent antitumor compound against A549 cancer cells (Thuan et al., 2017). In addition, the terpenoid humulene acts as a major bioactive component of balsam fir oil to inhibit tumours, including A549 cancer cells (Legault et al., 2003). Alpha-mangostin exhibited strong antitumor effects through ROS-mediated cytotoxicity in A549 cancer cells (Zhang *et al*., 2017). Lanosterol and cinnamaldehyde were also reported to inhibit A549 cancer cells (Chung et al., 2010; Wu et al., 2017). Some of these compounds also displayed antitumor properties and auxiliary functions in the treatment of cancer, of which quercetin 3-O-glucuronide, the only compound found in the mutant extracts, induced a ROS-dependent apoptosis pathway in MCF-7 cells (Wu et al., 2018), which indicated that AaLaeA mediated the production of this new compound. In our study, these compounds were significantly upregulated, which indicated that AaLaeA mediated the production of antitumor compounds.

Transcriptomic analysis was performed to reveal partial genes that might be involved in the biosynthesis of antitumor compounds. First, 66 related genes were screened and classified, including ABC transporters, PKSs, NRPSs, cytochrome P450s, GTs, the isoflavone reductase family, WD40 repeat-like proteins, and Myb transcription factors. A recent study showed that a putative ABC transporter formed a vital part of the nonribosomal peptide biosynthetic machinery (Gacek-Matthews et al., 2020), which indicated that ABC transporters are directly involved in secondary metabolite biosynthesis. In our study, ABC transporters were significantly enriched by GO and KEGG pathway analyses, suggesting that they greatly affected AaLaeA and might be involved in the synthesis of antitumor compounds. PKSs and NRPSs are large multimodule enzyme complexes involved in the biosynthesis of polyacetone and peptide secondary metabolites produced by microorganisms, such as bacteria and fungi (Singh et al., 2017). PKSA is a multidomain iterative PKS that catalyses the synthesis of aromatic polyketides (Crawford et al., 2008). It was upregulated 12-fold compared to the WT in our study. Additionally, the expression of the isoflavone reductase family was reported to be related to the accumulation of flavonoids (Hua et al., 2013), and the isoflavone reductase family protein-like protein CipA was upregulated up to 126-fold in the present study. Moreover, the expression of WD40 repeat-like proteins, Myb transcription factors and GTs are closely related to the biosythesis of flavonoids were also significantly upregulated or downregulated, of which GTs can affect glycosylated flavonoids, terpenoids, steroids and their biological activity; among these, flavonoids are the largest family of glycosylated secondary metabolites (Li et al 2018, Yang et al., 2019; Tiwari et al., 2016). Therefore, we proposed that these genes were important for the accumulation of polyketides, flavonoids and flavonoid glycosides (alpha-mangostin, myricetin, quercetin 3-O-glucuronide and others). Cytochrome P450s, haem-containing monooxygenases, are widely involved in the biosynthesis of secondary metabolites, including isoprenoids, steroids, flavonoids, alkaloids and phenolic compounds. Notably, some of the most important modification processes during the biosynthesis of terpenoids are catalysed mainly by cytochrome P450s (Zhang et al., 2021; Zheng et al., 2019). Therefore,

the transcriptome data showed that upregulation and downregulation of cytochrome P450s displayed the largest changes, suggesting that these enzymes were greatly affected by AaLaeA. Additionally, 29 genes were screened *via* integrated transcriptomic and metabolomic KEGG pathway analyses, including acetyl-CoA acetyltransferase, phosphomevalonate kinase, dehydrodolichyl diphosphate synthase, C-8 sterol isomerase, sterol C-24-methyltransferase, several hypothetical proteins, FAD binding domain-containing proteins and others. The mevalonate pathway is vital for the biosynthesis of steroids and terpenoids, and phosphomevalonate kinase and acetyl-CoA acetyltransferase are considered to be the key enzymes in this pathway (Wang et al., 2017). Additionally, dehydrodolichyl diphosphate synthase was proven to be the key enzyme in the synthesis of terpenoids (Cunillera et al., 2000), which were all upregulated in our study. Correspondingly, from the metabolomic analysis, the synthesis of terpenoids (humulene, geraniol and others) also showed a significant increase. Sterol C-24-methyltransferase is a key enzyme in the ergosterol biosynthesis pathway (Pereira et al., 2010), and the simultaneous overexpression of C-8 sterol isomerase and sterol C-24-methyltransferase significantly increases the ergosterol content (Zhang et al., 2009). In the same way, the expression of ergosterol in our research was also significantly increased. It is worth noting that hypothetical proteins and NAD/FAD-binding domain-containing proteins accounted for a large proportion of the 29 genes, with large changes in up-/downregulation. Therefore, these genes were most likely to be involved in the synthesis of antitumor compounds. In summary, the expression of the 95 identified genes was closely regulated after overexpression of *AalaeA* gene, and they might be responsible for the biosynthesis of antitumor compounds.

Our study revealed that AaLaeA mediates the antitumor activity of *A. alstroemeria* by regulating the expression of genes associated with secondary metabolism and antitumor substances in the strain. Nevertheless, our current research is limited, and the screened genes that may be related to secondary metabolites with antitumor properties await verification in the near future.

Declarations

Acknowledgements

Thanks to all authors for their contributions to this study.

Funding

This work was supported by the National Natural Science Foundation of China (No. 31670027, 32170019, 32160667, and 31901947).

Conflict of interest

The authors declare that they have no conflict of interest.

References

1. Ancheeva E, Daletos G, Proksch P (2020) Bioactive secondary metabolites from endophytic fungi. Curr Med Chem 27(11): 1836–1854
2. Anwar S, Khan S, Anjum F et al (2022) Myricetin inhibits breast and lung cancer cells proliferation via inhibiting MARK4. J Cell Biochem 123: 359–374
3. Bok JW, Keller NP (2004) LaeA, a regulator of secondary metabolism in *Aspergillus* spp. Eukaryot Cell 3: 527–535
4. Butchko RA, Brown DW, Busman M et al (2012) Lae1 regulates expression of multiple secondary metabolite gene clusters in *Fusarium verticillioides*. Fungal Genet Biol 49: 602–612
5. Christian N, Sedio BE, Florez-Buitrago X et al (2020) Host affinity of endophytic fungi and the potential for reciprocal interactions involving host secondary chemistry. Am J Bot 107: 219–228
6. Chung MJ, Chung CK, Jeong Y et al (2010) Anticancer activity of subfractions containing pure compounds of Chaga mushroom (*Inonotus obliquus*) extract in human cancer cells and in Balbc/c mice bearing Sarcoma-180 cells. Nutr Res Pract 4: 177–182
7. Crawford JM, Thomas PM, Scheerer JR et al (2008) Deconstruction of iterative multidomain polyketide synthase function. Science 320: 243–246
8. Crespo R, Rodenak-Kladniew BE, Castro MA et al (2020) Induction of oxidative stress as a possible mechanism by which geraniol affects the proliferation of human A549 and HepG2 tumor cells. Chem Biol Interact 320: 109029.
9. Cunillera N, Arró M, Forés O et al (2000) Characterization of dehydrodolichyl diphosphate synthase of Arabidopsis thaliana, a key enzyme in dolichol biosynthesis. FEBS Lett 477: 170–174
10. El Hajj Assaf C, Zetina-Serrano C, Tahtah N et al (2020) Regulation of Secondary Metabolism in the *Penicillium* Genus. Int J Mol Sci 21: 9462
11. Estiarte N, Lawrence CB, Sanchis V et al (2016) LaeA and VeA are involved in growth morphology, asexual development, and mycotoxin production in *Alternaria alternata*. Int J Food Microbiol 238: 153–164
12. Gacek-Matthews A, Chromikova Z, Sulyok M et al (2020) Beyond toxin transport: Novel role of ABC transporter for enzymatic machinery of cereulide NRPS assembly line. mBio 11: e01577-20
13. Gómez OC, Luiz JHH (2018) Endophytic fungi isolated from medicinal plants: future prospects of bioactive natural products from Tabebuia/Handroanthus endophytes. Appl Microbiol Biotechnol 102: 9105–9119
14. Hassan YA, Helmy MW, Ghoneim AI (2021) Combinatorial antitumor effects of amino acids and epigenetic modulations in hepatocellular carcinoma cell lines. Naunyn Schmiedebergs Arch Pharmacol 394: 2245–2257
15. He Z, Luo L, Keyhani NO, et al (2017) The c-terminal mir-containing region in the pmt1 o-mannosyltransferase restrains sporulation and is dispensable for virulence in *beauveria bassiana*. Appl Microbiol Biotechnol 101: 1–19

16. Hong EJ, Kim NK, Lee D et al (2015) Overexpression of the laeA gene leads to increased production of cyclopiazonic acid in *Aspergillus* fumisynnematus. Fungal Biol 119: 973–983
17. Hridoy M, Gorapi MZH, Noor S et al (2022) Putative anticancer compounds from plant-derived endophytic fungi: a review. Molecules 27: 296
18. Hua C, Lingling L, Feng X et al (2013) Expression patterns of an isoflavone reductase-like gene and its possible roles in secondary metabolism in Ginkgo biloba. Plant Cell Rep 32: 637–650.
19. Huang SF, Horng CT, Hsieh YS et al (2016) Epicatechin-3-gallate reverses TGF-beta1-induced epithelial-to-mesenchymal transition and inhibits cell invasion and protease activities in human lung cancer cells. Food Chem Toxicol 94: 1–10.
20. Jiang T, Wang M, Li L et al (2016) Overexpression of the global regulator LaeA in *Chaetomium globosum* leads to the biosynthesis of Chaetoglobosin Z. J Nat Prod 79: 2487–2494
21. Jung YY, Hwang ST, Sethi G et al (2018) Potential anti-inflammatory and anti-cancer properties of farnesol. Molecules 23: 2827
22. Legault J, Dahl W, Debiton E et al (2003) Antitumor activity of balsam fir oil: production of reactive oxygen species induced by alpha-humulene as possible mechanism of action. Planta Med 69: 402–479
23. Li Y, Fang J, Qi X et al (2018) Combined analysis of the fruit metabolome and transcriptome reveals candidate genes involved in flavonoid biosynthesis in *actinidia arguta*. Int J Mol Sci 19: 1471
24. Liu T, Li Y, Sun J et al (2020) Engeletin suppresses lung cancer progression by inducing apoptotic cell death through modulating the XIAP signaling pathway: A molecular mechanism involving ER stress. Biomed Pharmacother 128: 110221
25. Liu YP, Pu CJ, Wang M et al (2019) Cytotoxic ergosterols from cultures of the basidiomycete Psathyrella candolleana. Fitoterapia 138: 104289
26. Lu XJ, Chen SF, Xu XW et al (2018) One pair of new cyclopentaisochromenone enantiomer from *Alternaria* sp. TNXY-P-1 and their cytotoxic activity. J Asian Nat Prod Res 20: 328–336
27. Ma GL, Guo N, Wang XL et al (2020) Cytotoxic secondary metabolites from the vulnerable conifer cephalotaxus oliveri and its associated endophytic fungus *Alternaria* alternate Y-4-2. Bioorg Chem 105: 104445
28. Macheleidt J, Mattern DJ, Fischer J et al (2016) Regulation and Role of Fungal Secondary Metabolites. Annu Rev Genet 50: 371–392
29. Martin JF (2017) Key role of LaeA and velvet complex proteins on expression of beta-lactam and PR-toxin genes in *Penicillium chrysogenum*: cross-talk regulation of secondary metabolite pathways. J Ind Microbiol Biotechnol 44: 525–535
30. Nishikawa J and Nakashima C (2013) Taxonomic characterization and experimental host ranges of four newly recorded species of *alternaria* from Japan. J Phytopathol 61: 604–616
31. Pereira M, Song Z, Santos-Silva LK et al (2010) Cloning, mechanistic and functional analysis of a fungal sterol C24-methyltransferase implicated in brassicasterol biosynthesis. Biochim. Biophys

Acta 1801: 1163–1174

32. Pu J, Tang X, ZhuangX et al (2018) Matrine induces apoptosis via targeting CCR7 and enhances the effect o f anticancer drugs in non-small cell lung cancer in vitro. Innate Immun 24: 394–399
33. Shwab EK and Keller NP (2008) Regulation of secondary metabolite production in filamentous ascomycetes. Mycol Res 112: 225–230
34. Singh M, Chaudhary S, and Sareen D (2017) Non-ribosomal peptide synthetases: Identifying the cryptic gene clusters and decoding the natural product. J Biosci 42: 175–187
35. Su CC, Hsieh KL, Liu PL et al (2019) AICAR induces apoptosis and inhibits migration and invasion in prostate cancer cells through an AMPK/mTOR- dependent pathway. Int J Mol Sci 20: 1647
36. Sun R, Man Z, Ji J et al (2020) L-Carnitine protects against 1, 4-benzoquinone- induced apoptosis and DNA damage by suppressing oxidative stress and promoting fatty acid oxidation in K562 cells. Environ Toxicol 35: 1033–1042
37. Thuan NH, Malla S, Trung NT et al (2017) Microbial production of astilbin, a bioactive rhamnosylated flavanonol, from taxifolin. World J Microbiol Biotechnol 33: 36
38. Tian J, Fu L, Zhang Z et al (2017) Dibenzo-alpha-pyrones from the endophytic fungus *Alternaria* sp. Samif01: isolation, structure elucidation, and their antibacterial and antioxidant activities. Nat Prod Res 31: 387–396
39. Tiwari P, Sangwan RS, and Sangwan NS (2016) Plant secondary metabolism linked gly cosyltransferases: An update on expanding knowledge and scopes. Biotechnol Adv 34: 714–739
40. Tsai CM, Sun FM, Chen YL et al (2013) Molecular mechanism depressing PMA-induced invasive behaviors in human lung adenocarcinoma cells by cis- and trans-cinnamic acid. Eur J Pharm Sci 14: 494–501
41. Wang M, Wang D, Zhang Q et al (2017) Identification and cytochemical immunolocalization of acetyl-CoA acetyltransferase involved in the terpenoid mevalonate pathway in euphorbia helioscopia laticifers. Bot Stud 58: 62
42. Williams RB, Henrikson JC, Hoover AR et al (2008) Epigenetic remodeling of the fungal secondary metabolome. Org Biomol Chem 6: 1895–1897
43. Wu C, Zhuang Y, Jiang S et al (2017) Cinnamaldehyde induces apoptosis and reverses epithelial-mesenchymal transition through inhibition of Wnt/β-catenin pathway in non-small cell lung cancer. Int J Biochem Cell Biol 84: 58–74
44. Wu CS, Chen YJ, Chen JJ et al (2012) Terpinen-4-ol induces apoptosis in human nonsmall cell lung cancer in vitro and In vivo. Evid. Based Complement. Alternat Med 2012: 818261
45. Wu Q, Needs PW, Lu Y et al (2018) Different antitumor effects of quercetin, quercetin-3'-sulfate and quercetin-3-glucuronide in human breast cancer MCF-7 cells. Food Funct 9: 1736–1746
46. Xie J, Liu J, Liu H et al (2015) The antitumor effect of tanshinone IIA on anti-proliferation and decreasing VEGF/VEGFR2 expression on the human non-small cell lung cancer A549 cell line. Acta Pharm Sin B 5: 554–563

47. Yan L, Zhao H, Zhao X et al (2018) Production of bioproducts by endophytic fungi: chemical ecology, biotechnological applications, bottlenecks, and solutions. Appl Microbiol Biotechnol 102: 6279–6298
48. Yang M, Zhou P, Gui C et al (2019) Comparative transcriptome analysis of ampelopsis megalophylla for identifying genes involved in flavonoid biosynthesis and accumulation during different seasons. Molecules 24: 1267
49. Yu J, Han H, Zhang X et al (2019) Discovery of two new sorbicillinoids by overexpression of the global regulator LaeA in a marine-derived fungus *Penicillium dipodomyis* YJ-11. Mar Drugs 17: 446
50. Zhang C, Yu G, and Shen Y (2018) The naturally occurring xanthone alpha-mangostin induces ROS-mediated cytotoxicity in non-small scale lung cancer cells. Saudi J Biol Sci 25: 1090–1095
51. Zhang C, Zhang H, Zhu Q et al (2020) Overexpression of global regulator LaeA increases secondary metabolite production in *Monascus purpureus*. Appl Microbiol Biotechnol 104: 3049–3060
52. Zhang X, Guo J, Cheng F et al (2021) Cytochrome P450 enzymes in fungal natural product biosynthesis. Nat Prod Rep 38: 1072–1099
53. Zhang Z, He X, Li W et al (2009) Regulation role of sterol C-24 methyltransferase and sterol C-8 isomerase in the ergosterol biosynthesis of Saccharomyces cerevisiae. Wei Sheng Wu Xue Bao 49: 1063–1068
54. Zheng X, Li P, and Lu X (2019) Research advances in cytochrome P450-catalysed pharmaceutical terpenoid biosynthesis in plants. J Exp Bot 70: 4619–4630
55. Zhu X, Li H, Long L et al (2012) miR-126 enhances the sensitivity of non-small cell lung cancer cells to anticancer agents by targeting vascular endothelial growth factor A. Acta Biochim. Biophys Sin (Shanghai) 44: 519–526

Figures

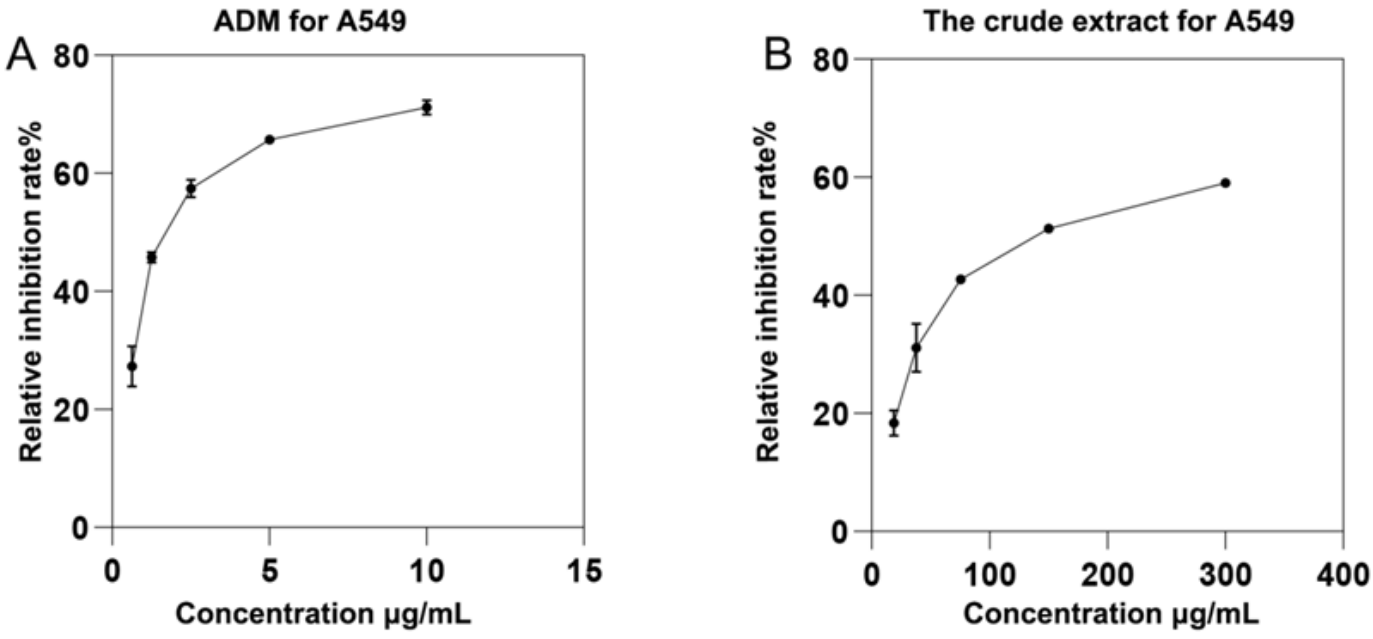

Figure 1

Effects of ADM and A. alstroemeria extract on the A549 cancer cell line. A549 cancer cells were seeded at a density of 1×105 cells/well and treated with different concentrations of ADM or A. alstroemeria extract for 48 h; three replicates were performed for each concentration. An MTT assay was conducted to determine the cellular proliferation inhibition rate. A. Relative inhibition rates of A549 cancer cells after treatment with 0.625, 1.25, 2.5, 5 and 10 μg/mL ADM. Each point on the graph represents the mean ± SD of triplicate tests. B. Relative inhibition rates of A549 cancer cells after treatment with 18.75, 37.5, 75, 150 and 300 μg/mL extract. Values represent the mean±SD of 3 replicates per treatment.

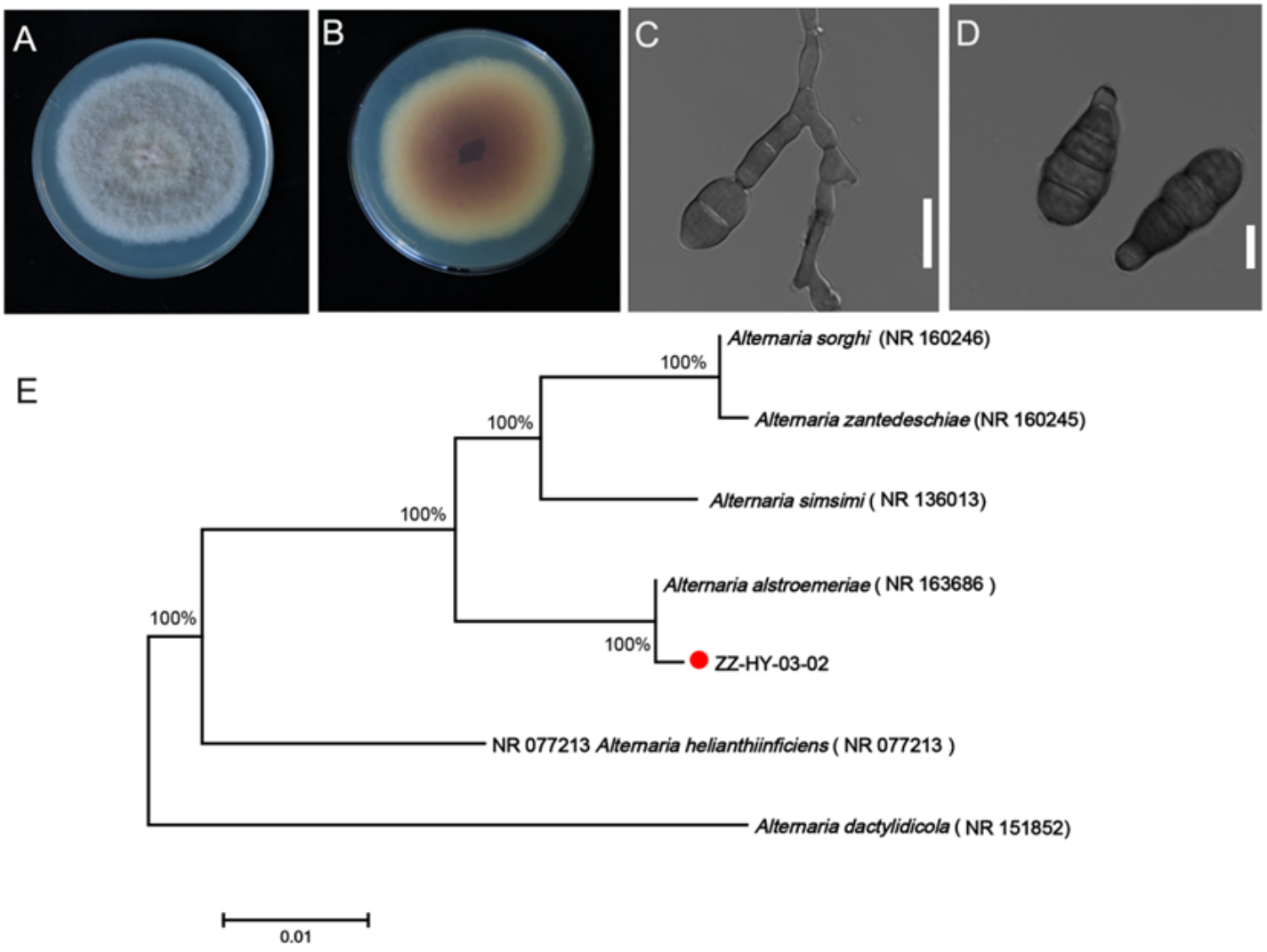

Figure 2

Morphological characteristics and ITS phylogenetic analysis of the fungus ZZ-HY-03-02. A. Growth on PDA plates. The colonies were cultivated at 28 °C for 6 days. B. The back of the PDA medium. C. Microscopic image of conidiophores ((scale: 10 μm). D. Microscopic image of the conidia (scale: 10 μm)). E. Phylogenetic tree constructed based on the ITS genes of the members of the *Alternaria* genus

using the maximum likelihood (ML) method with 1000 bootstrap replicates. Numbers in parentheses are the GenBank accession numbers of published sequences. *A. dactylidicola* was used as the outgroup, and the red circle represents the strain identified in the study.

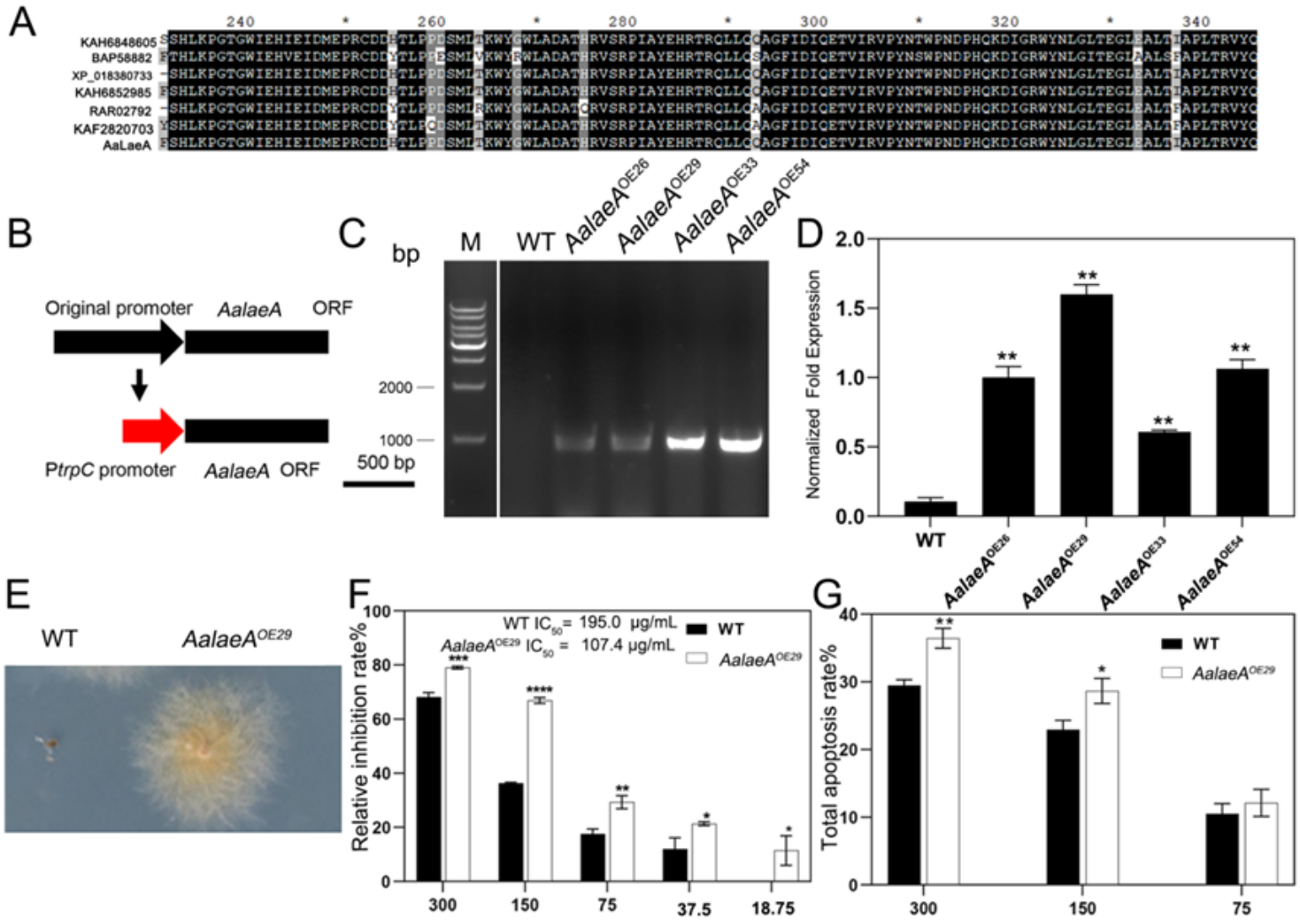

Figure 3

Identification of the AaLaeA protein, design of the transformation vectors, verification of the positive transformants and determination of A549 cancer cell proliferation and apoptosis. A. Protein sequence alignment of LaeA in *A. alstroemeria.* Multiple sequence alignment was performed using the Clustal W alignment algorithm with Mega 7.0 and edited with GeneDoc version 6. B. Schematic of the mutant vector construction. The original promoter of the ORF of the *AalaeA* gene was replaced by the constituent promoter *PtrpC* of *Aspergillus nidulans* to drive the expression of *AalaeA* (scale: 500 bp). C. Amplification of the *hyg* gene to verify the transformants. Four transformants were selected to amplify the *hyg* gene with the primers *hyg*-F and *hyg*-R primers (M: Star Marker D2000 (Genstar, Beijing, China), *AalaeA*^{OE29}, *AalaeA*^{OE26}, *AalaeA*^{OE33} and *AalaeA*^{OE54} were the randomly selected transformants). D. Expression level of the *laeA* gene in the WT and the mutant strains. qRT–PCR was used to evaluate the expression of *AalaeA*

in the WT and transformants *AalaeA*^{OE29}, *AalaeA*^{OE26}, *AalaeA*^{OE33} and *AalaeA*^{OE54}. E. The state of the WT and *AalaeA*^{OE29} strains on hygromycin B-resistant CZM plates (100 μg/mL). AalaeAOE29 grew normally on hygromycin B resistant plates (100 μg/mL), while WT growth was inhibited. F. Effects of the of WT and AalaeAOE29 extracts on A549 cancer cells proliferation. A549 cancer cells were seeded at a density of 1×10^5 cells/well in 96-well plates and treated with WT *and AalaeA*^{OE29} extracts at concentrations of 18.75, 37.5, 75, 150 and 300 μg/mL for 48 h; three replicates were set for each concentration. MTT assays detected the inhibition of A549 cancer cell proliferation induced by extract treatment. Statistical differences from WT: $^{*}(P < 0.05)$, $^{**}(P < 0.01)$,$^{***}(P < 0.005)$, $^{****}(P < 0.001)$ G. Cell apoptosis effects induced by the WT and *AalaeA*^{OE29} extracts in the A549 cancer cell line. A549 cancer cells were seeded at a density of 1×10^6 cells/well in 6-well plates and treated with 75, 150 and 300 μg/ml WT *and AalaeA*^{OE29} extracts for 48 h. Annexin V-FITC/PI double staining was used to detect apoptosis. Values represent the mean±SD of 3 replicates per treatment. $^{*}(P < 0.05)$, $^{**}(P < 0.01)$.

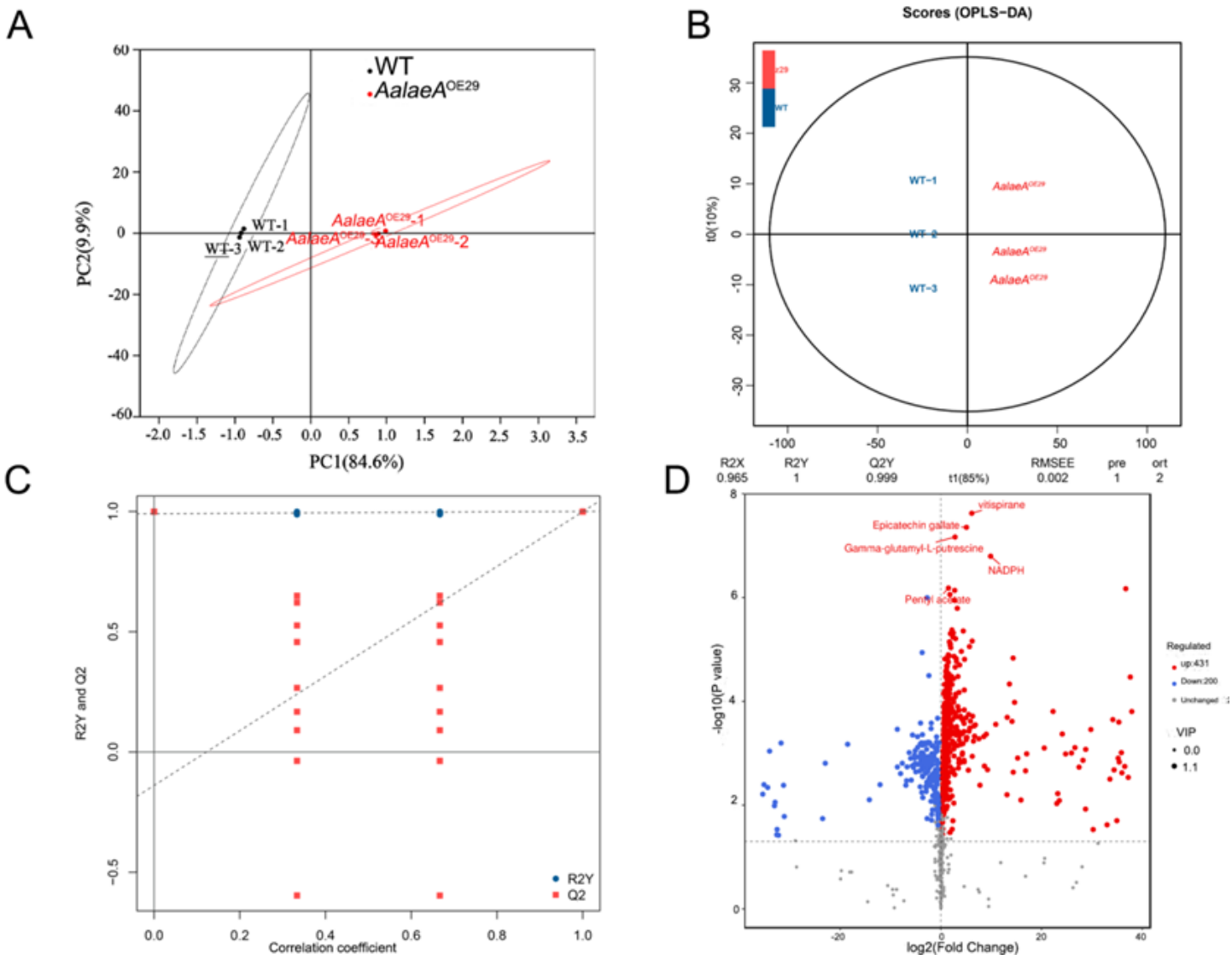

Figure 4

An overview of the metabolite distribution in the WT and *AalaeA*^{OE29} strains. A. PCA distribution map of metabolites. Black and red dots represent WT and *AalaeA*^{OE29}, respectively, from three replicate groups; the three groups had good repeatability. The first two principal components accounted for 94.5% of the overall variability, with PC1 accounting for 84.6% of the variance and PC2 accounting for 9.9%. B. OPLS-DA score plot. The two groups of data were clearly separated without outliers. The blue and red dots represent WT and *AalaeA*^{OE29}, respectively, from three replicate groups, all of which were within the 95% confidence interval (Hotelling's T-squared ellipse). C. Permutation test of the OPLS-DA model. The ordinate is the R2Y or Q2 value, and the blue dot is the R2Y value from the substitution test. The red square represents the value of Q2 obtained by the substitution test, and the two dotted lines represent the regression lines of R2Y and Q2. D. Each dot represents a metabolite. Blue represents downregulation, red represents upregulation, and grey represents unchanged expression. The abscissa shows multiple change values (log2 fold changes) in the comparison material group, and the ordinate shows the P value from Student's t test (−log10 P value). The point size represents the VIP value from the OPLS-DA model. The larger the scatter is, the greater the VIP value.

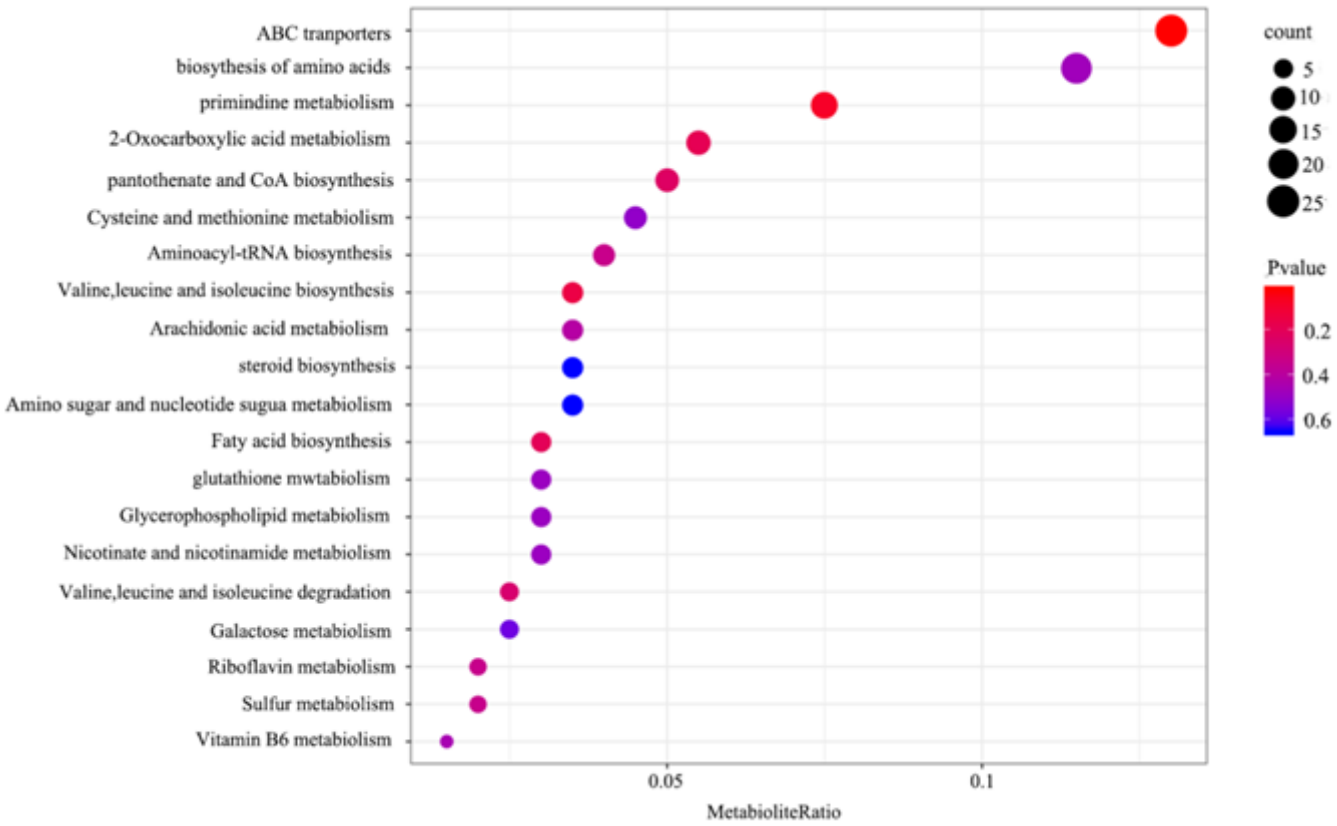

Figure 5

The pathways in which the metabolites are involved determined by KEGG enrichment pathway analysis. A KEGG pathway bubble diagram is shown. Each bubble represents a metabolic pathway, the abscissa displays the metabolite ratio, the ordinate shows the enrichment pathways of the metabolites, the sizes of the bubbles represent the gene counts, and the colour scale reflects the P value.

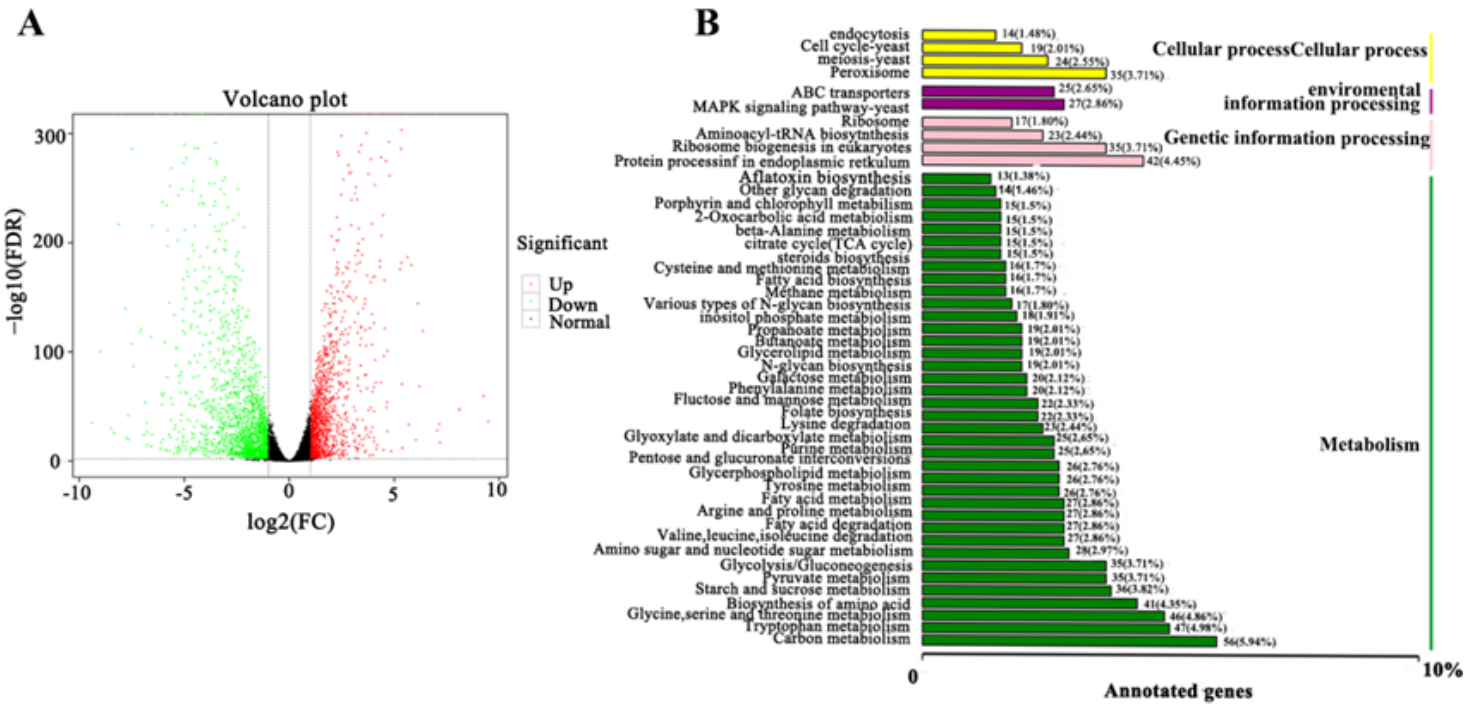

Figure 6

Volcano plot and classification of the KEGG pathways of the 3648 DEGs. A. Volcano plot showing the DEGs that matched the criteria of FC ≥ 1, FDR ≤ 0.05, and VIP > 1.0. The red plot represents unregulated genes, the green plot represents downregulated genes, and the grey plot represents genes with unchanged expression. B. Classification of the KEGG pathways. The ordinate is the grouping of the genes, the yellow, purple, pink and green columns represent “cell process”, “environmental information processing”, “genetic information processing” and “metabolism”, respectively, and the abscissa is the ratio of genes annotated to this pathway to the total pathway genes.

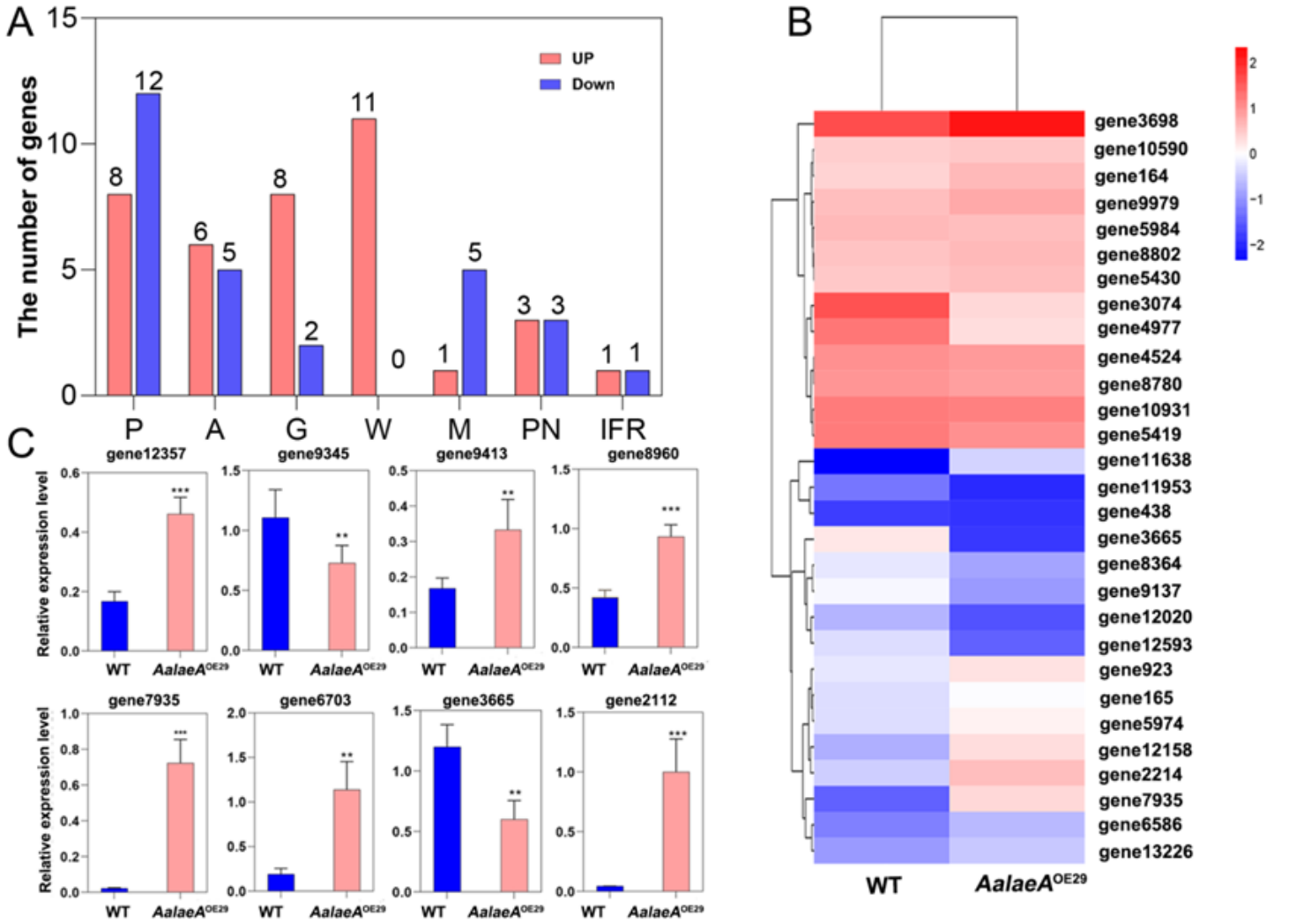

Figure 7

Expression of the 95 DEGs involved in the biosynthesis of antitumor compounds and qRT–PCR validation of thetranscriptome data. A. The 66 upregulated and downregulated DEGs, including the enzymes, proteins, and transcription factors that are closely related to the biosynthesis of the antitumor compounds (P, A, G, W, M, PN, and IFR represent cytochrome P450s, ABC transporters, GTs, WD40 repeat-like proteins, Myb transcription factors, PKSs and NRPSs, and isoflavone reductase family members, respectively). B. Expression patterns of the 29 DEGs involved in the biosynthesis of steroids, terpenoids and various secondary metabolites. Hierarchical clustering of the enriched DEGs combined with transcriptomic and metabolomic KEGG pathway analyses. Blue and red represent different levels of gene expression, and the colour scales reflect the log2-transformed mean of the fragments per kilobase of transcript per million mapped (FPKM) values. C. Eight DEGs in the transcriptomic analysis were selected for transcriptome data verification. Relative gene expression was normalized to the expression of actin and calculated using the $2^{-\triangle\triangle Ct}$ method. Values represent the mean±SD of 3 replicates per treatment $^{*}(P < 0.05)$, $^{**}(P < 0.01)$,$^{***}(P < 0.005)$.

Supplementary Files

This is a list of supplementary files associated with this preprint. Click to download.

- AMSupplementarymaterial.docx